# Electronic Supplementary Information (ESI)

## In-chain functionalized polymers induced assembly of nanoparticles: toward materials with tailored properties

Li Liu,[a] Chongzhi Sun,[a] Ziwei Li,[a] Yulong Chen,[b,*] Xin Qian,[b] Shipeng Wen[c,d] and Liqun Zhang[c,d]

[a] State Key Laboratory of Chemical Resource Engineering, Beijing University of Chemical Technology, Beijing 100029, China.

[b] College of Materials Science and Engineering, Zhejiang University of Technology, Hangzhou 310014, China. E-mail: chenyulong@zjut.edu.cn

[c] State Key Laboratory of Organic-Inorganic Composites, Beijing University of Chemical Technology, Beijing 100029, China.

[d] Beijing Engineering Research Center of Advanced Elastomers, Beijing University of Chemical Technology, Beijing 100029, China.

**Method Section**

*Simulation method*

In our simulations, the in-chain functionalized polymers with chain length $N$ = 65 were modeled as bead–spring chains without explicit twisting or bending potential, and each consisting of two types of monomers (type A and B) with diameters $\sigma$ and masses $m$, where the B monomers were used to represent functionalized monomers that are uniformly distributed within the polymer chains. Each chain consisting of monomers was connected by anharmonic springs modeled with a stiff finite extensible nonlinear elastic (FENE) potential[1]

$$V_{\mathrm{FENE}} = -0.5kR_0^2 \ln\left[1-\left(\frac{r}{R_0}\right)^2\right] \tag{S1}$$

where $k = 30\varepsilon/\sigma^2$ is the spring constant and $R_0 = 1.5\sigma$ is the maximum extent of the bond. Note that all quantities were measured in reduced Lennard-Jones (LJ) units, i.e., distance, mass, and energy were measured in units of $\sigma$, $m$, and $\varepsilon$, respectively. The nanoparticles (NPs) were represented by LJ spheres with diameters ($D_{\mathrm{NP}}$) equal to $4\sigma$ and masses equal to $64m$. The non-bonded interactions between all interacting sites (including polymer monomers and NPs) were described by using a modified LJ potential[2]

$$U_{i-j}(r) = \begin{cases} 4\varepsilon_{i-j}\left[\left(\frac{\sigma}{r_{i-j}-\Delta_{i-j}}\right)^{12} - \left(\frac{\sigma}{r_{i-j}-\Delta_{i-j}}\right)^{6}\right] - U(r_{cutoff}) & 0 < r_{i-j}-\Delta_{i-j} < r_{cutoff} \\ 0 & r_{i-j}-\Delta_{i-j} \geq r_{cutoff} \end{cases} \tag{S2}$$

where $\varepsilon_{i-j}$ and $r_{i-j}$ are the energy parameter and the distance, respectively, between interacting sites $i$ and $j$. The interaction range was offset by $\Delta_{i-j}$ to account for the excluded volume effect of the two interacting sites, and $r_{cutoff}$ is the distance $r_{i-j}-\Delta_{i-j}$ at which the potential is truncated

and shifted. For interactions between polymer monomers, the energy parameter $\varepsilon_{\mathrm{P-P}}$ was set to $\varepsilon$ with a zero value for $\Delta_{\mathrm{P-P}}$, and the cut-off distance was taken as $r_{cutoff} = 2 \times 2^{1/6}\sigma$ to include the attractive portion. The NP–NP interactions with $\varepsilon_{\mathrm{NP-NP}}$ equal to $\varepsilon$ and $\Delta_{\mathrm{NP-NP}}$ equal to $3\sigma$ were truncated and shifted at $r_{cutoff} = 2.5\sigma$ to take into account the weakly attractive interactions between NPs. The interactions between A monomers and NPs were set to be purely repulsive such that A monomers are immiscible with NPs, i.e., the interactions with $\varepsilon_{\mathrm{A-NP}} = \varepsilon$ and $\Delta_{\mathrm{A-NP}} = 1.5\sigma$ were truncated and shifted at $r_{cutoff} = 2^{1/6}\sigma$. To mimic the strong affinity of B monomers for NPs, the energy parameter $\varepsilon_{\mathrm{B-NP}}$ was set to $10\varepsilon$ with $\Delta_{\mathrm{B-NP}} = 1.5\sigma$, and the cutoff distance was taken as $r_{cutoff} = 2.5\sigma$.

In each system, the total number of polymer monomers was fixed at 13000, and the number density of polymer monomers was held near $\rho^* = 0.85$. The functionalization degree $d_{\mathrm{B}} = N_{\mathrm{B}}/(N_{\mathrm{A}}+N_{\mathrm{B}})\times 100\%$ was varied from 0.00% to 30.8%, where $N_{\mathrm{A}}$ and $N_{\mathrm{B}}$ are the numbers of A and B monomers in a chain, respectively. The number of added NPs ($N_{\mathrm{NP}}$) was varied from 30 to 150. The volume fraction of NPs, defined by $\phi_{\mathrm{NP}} = N_{\mathrm{NP}} 4\pi D_{\mathrm{NP}}^3 / 3L^3 \times 100\%$, where $L$ is the box length, was varied from 6.17 vol% to 24.74 vol%. For the above systems, we performed NVT simulations using Nosé–Hoover thermostat to maintain constant temperature $T^* = 1.0$. Periodic boundary condition was employed in all three directions of the simulation box. The velocity-Verlet algorithm was applied to integrate the equations of motion with a time step of $\delta t^* = 0.001$, where the time was reduced by the LJ time ($\tau$).

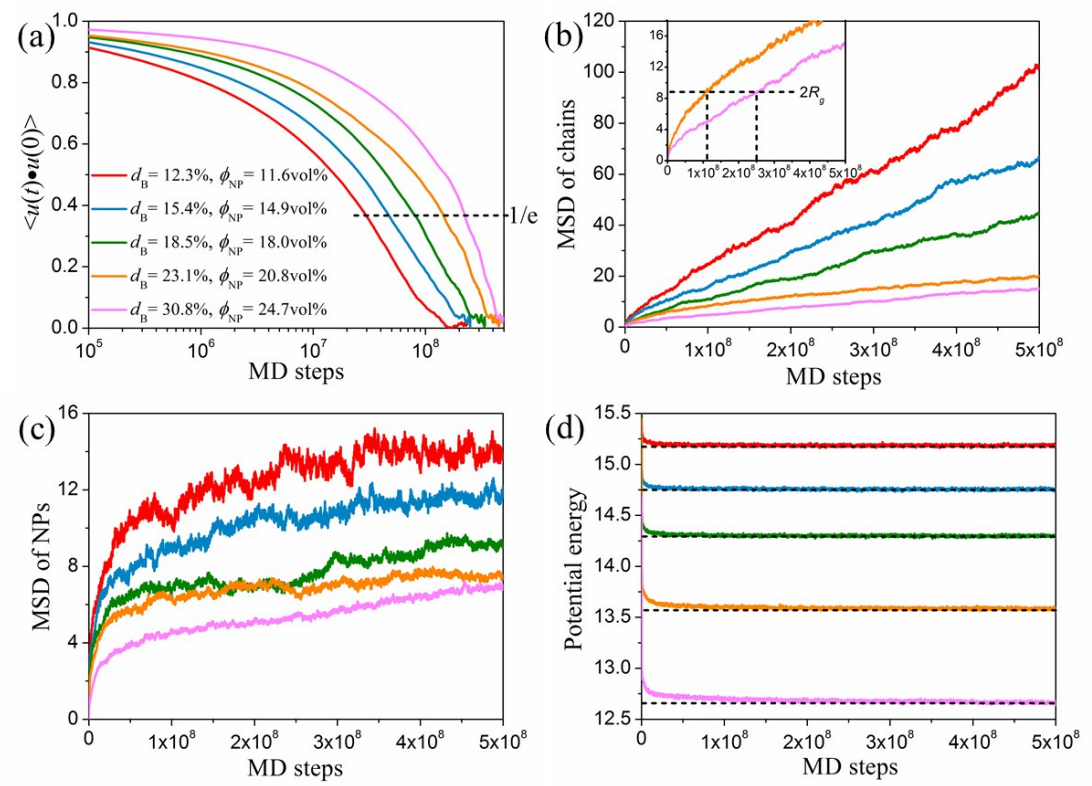


**Fig. S1** (a) the end-to-end vector autocorrelation function $\langle u(t) \bullet u(0) \rangle$, (b) mean-square displacement (MSD) of polymer chains, (c) MSD of NPs, and (d) the potential energy of the systems as a function of MD steps.

Initially, randomly generated polymer/NP mixtures were equilibrated with only purely repulsive LJ interactions. Then we switched on the interactions between different pairs and let the systems equilibrate for a long time ($3.0 \times 10^8$ MD steps). To make sure whether the systems reached equilibrium, the relaxation of polymer chains, the mean-square displacements (MSDs) of chains and NPs, the potential energy of the systems during MD runs were monitored. The longest relaxation of polymer chains can be characterized by the end-to-end vector autocorrelation function $\langle u(t) \bullet u(0) \rangle$, with $u(t)$ being the unit vector along the end-to-end vector of a chain, and its decay rate can reflect how fast polymer chain forgets its initial configuration, as shown in Fig. S1a. It is found that after long-time simulations, the end-to-end vector autocorrelation function is decay to a value below 1/e. Meanwhile, the polymer chains and the

NPs also reach the diffusive regime (Fig. S1b and Fig. S1c). The polymer chains have moved at least $2R_g$ (Fig. S1b), and the potential energy is steady (Fig. S1d). Therefore, $3.0 \times 10^8$ time-steps is long enough to ensure the equilibrium of these systems.

In this work, all the MD simulations are carried out using the open source LAMMPS molecular dynamics package.[3] Ten independent simulations were performed for each system, and $10^4$ final configurations were dumped at every $10^3$ time-steps (corresponding to a time interval of $1\,\tau$) after the simulations were equilibrium.

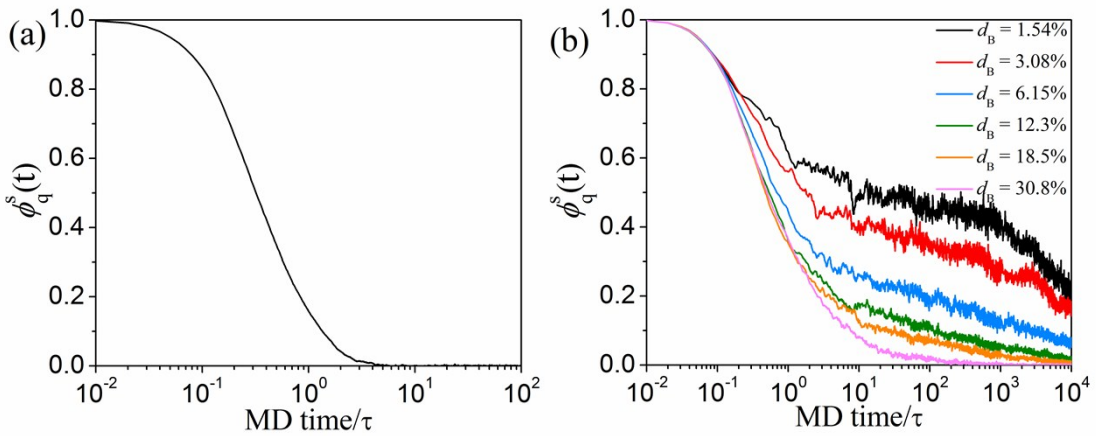


**Fig. S2** Incoherent intermediate dynamic structure (IIDS) factor $\phi_q^s(t)$ as a function of time (a) for the segmental relaxation behavior of pure polymer (of chain length $N = N_e = 35$) and (b) for the relaxation behavior of B monomers adsorbed on NPs for the systems with $\phi_{NP} = 11.62\%$ at different functionalization degrees.

The algorithm for the steady shear was realized using the SLLOD equations of motion,[4,5] which was implemented through a continuously deforming, non-orthogonal simulation box.[6] By shifting the upper *xz* plane of the simulation box along the *x*-axis direction, a steady linear velocity profile with a gradient of $\partial V_x / \partial y$ along the *y* direction was applied to the simulation box, where $V_x$ is the velocity along the shear direction (*x*-axis). The shear rate, defined as $\dot{\gamma} = \partial V_x / \partial y$, was set to $0.01\,\tau^{-1}$; that is, the shear strain will increase by 0.01 per unit time. We

have compared this shear rate with the simulated segmental relaxation time $\tau_s$ and Rouse time $\tau_R$ of pure polymer (of length $N = N_e = 35$, where $N_e$ is the entanglement length for this model). The segmental relaxation behavior were determined by the incoherent intermediate dynamic structure (IIDS) factor $\phi_q^s(t)$ from the relationship,[7-9]

$$\phi_q^s(t) = \frac{1}{M}\sum_{i=1}^{M}\left\{\exp\left\langle \mathbf{iq}\cdot\left[\mathbf{r}_i(t)-\mathbf{r}_i(0)\right]\right\rangle\right\} \quad \text{(S3)}$$

where $M$ stands for the total number of monomers in the polymer, ($\mathbf{r}_i$(t)- $\mathbf{r}_i$(0)) is the displacement of the scattering center $i$ after time $t$, and **q** is the momentum transfer and its values is equal to 6.9 when use IIDS to probe the segmental relaxation. As shown in Fig. S2a, the segmental relaxation time is less than $5\tau$. The Rouse time $\tau_R$ is determined from $\tau_R = (1/3\pi^2)\cdot 6\left\langle R_g^2\right\rangle / D_R$,[10] where $D_R$ is the Rouse self-diffusion constant obtained by $D_R = \lim_{t\to\infty}\left\langle \mathbf{r}_{cm}(t)-\mathbf{r}_{cm}(0)\right\rangle^2 / 6t$,[11] where ($\mathbf{r}_{cm}$(t)- $\mathbf{r}_{cm}$(0)) is the displacement of the center-of-mass of polymer chains after time $t$. We find that $\tau_R = 1.3\times10^5\tau$. Therefore, $\dot{\gamma}\tau_s < 1$ and $\dot{\gamma}\tau_R > 1$. This condition could ensure the sheared-systems not to be under glassy state but the shear force still strong enough to orient and stretch the polymer chains. In addition, we also monitored the relaxation behavior of B monomers adsorbed on NPs (those within a distance of $3.0\sigma$ to the center-of-mass of the NPs), as shown in Fig. S2b. We find that the time scale of shear rate is smaller than the adsorption time of the functional monomers, promising the ability of NP-mediated polymer network to hold the shear force. All the above findings suggest that the shear rate adopted in this study is reasonable. Each system was sheared for $4\times10^6$ steps, and the stress response at each time step was collected. Then, the shear stress $\sigma_{xy}$ can be obtained from the deviatoric part of the stress tensor $\sigma_{xy} = P_{xy} = P_{yx}$.[12]

*Calculations of directly-connected-NP clusters and probability of their percolating network*

Based on the result configurations, a statistical analysis of the sizes and numbers of directly-connected-NP clusters was performed. Here, the size of a cluster is defined as the number of NPs within the cluster. Before implementing the analysis, each NP was assigned a unique ID number increasing from 1 to $N_{NP}$. Then the connection between these NPs was checked. If two NPs were attached to each other within a distance of $4.5\sigma$, they got the same ID number that was the smaller of the two ID numbers of these NPs. Once the entire system was scanned, all particles that have the same ID number are in the same cluster. Consequently, particles with different ID numbers were not connected. If a ID number labels only one particle, this particle is in isolated state. Once the network of particles spans three-dimensional directions continuously, the system is percolating. The probability of percolating network formation is calculated by the ratio of the number of the percolating configurations to that of all the configurations obtained from the ten independent simulations of each system.

**Movies**

**Movie S1** The assembly process of system with filler volume fraction $\phi_{NP}$ = 11.62 vol% and functionalization degree $d_B$ = 1.54%.

**Movie S2** The assembly process of system with filler volume fraction $\phi_{NP}$ = 11.62 vol% and functionalization degree $d_B$ = 3.08%.

**Movie S3** The assembly process of system with filler volume fraction $\phi_{NP}$ = 11.62 vol% and functionalization degree $d_B$ = 6.15%.

**Movie S4** The assembly process of system with filler volume fraction $\phi_{NP}$ = 11.62 vol% and functionalization degree $d_B$ = 30.8%.

**Some Additional Analyses**

*The steric effect*

On the basis of an integral equation theory of the microscopic polymer reference interaction site model (PRISM), Hooper and Schweizer[13] studied the microstructures of polymer and particles in nanocomposite melts. They established the conditions on the strength and spatial range of polymer−particle attractive interactions that defined four different modes of NP organization: (i) contact aggregation, (ii) steric stabilization due to thermodynamically stable "bound polymer layers", (iii) segmental-level tight particle bridging, and (iv) "tele-bridging". These theoretical results were also found in many resent MD studies.[14,15]

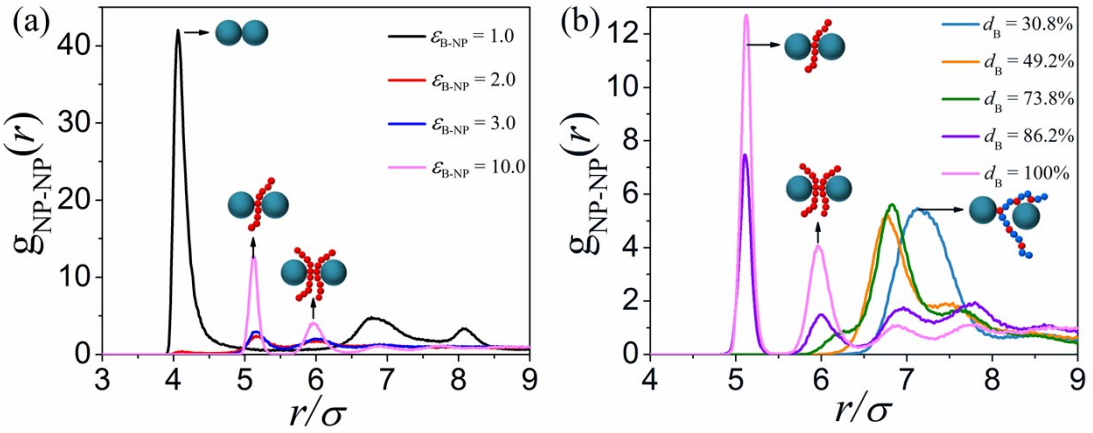


**Fig. S3** Radial distribution function of NPs, $g_{NP\text{-}NP}(r)$, (a) for systems with $d_B$ = 100% but at different B–NP interactions and (b) for systems with a fixed B–NP interaction $\varepsilon_{B\text{–}NP}$ = 10.0 but at different $d_B$. The filler loading for each system is fixed at $\phi_{NP}$ = 11.62 vol%.

Here, some additional simulations were also carried out to verify the above findings. In these simulations, all polymer sites are attractive with NPs. At a low polymer–NP interaction such as $\varepsilon_{B\text{–}NP}$ = 1.0, a peak appears at $r = 4\sigma$, indicating direct contact aggregation of the fillers (Fig. S3a). If the interaction increases to 2.0, the peaks appear at $r = 5\sigma$ and $6\sigma$, which suggests that the NPs tend to form aggregates sandwiched by one or two polymer layers, as schematically

shown in Fig. S3a. The peaks at $r = 5\sigma$ and $6\sigma$ become higher with the increasing interaction, meaning the more NPs tend to aggregate via polymer chains.

However, the NPs aggregate through the bridging mechanism does not observed for $d_B$ = 30.8%, where the B monomers are uniformly distributed within polymer chains. It is also the case for $d_B$ = 49.2% (Fig. S3b). This is due to the steric effect of A blocks that connected to the B monomers, as schematically shown in Fig. S3b. If $d_B$ further increased ($d_B$ > 73.8%), the bridging mechanism should occur (Fig. S3b).

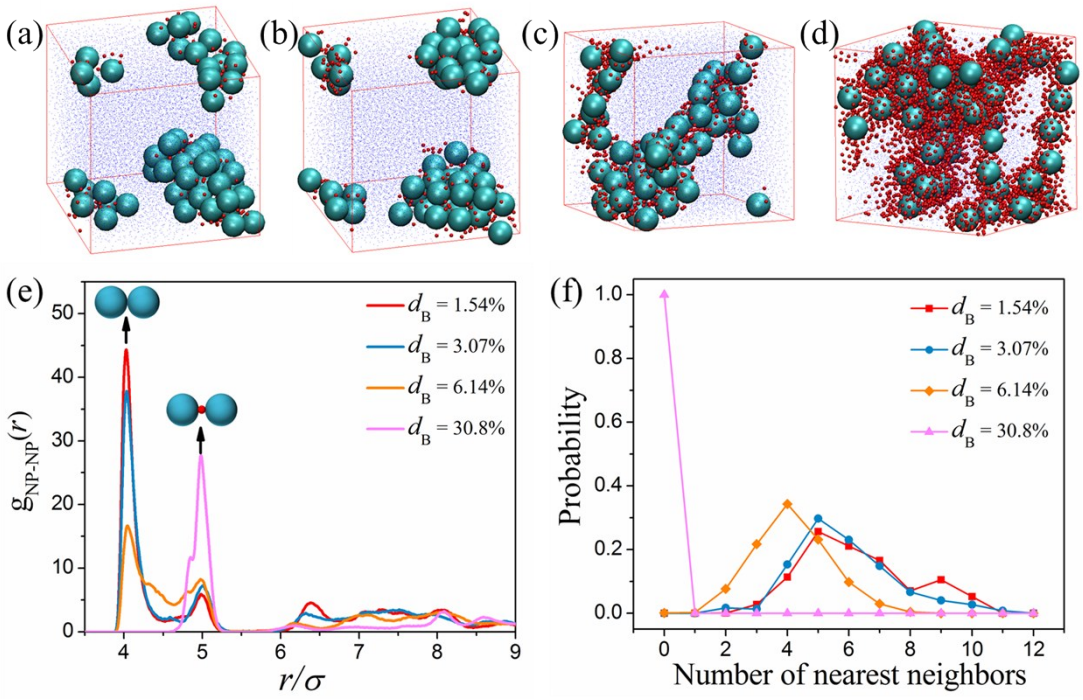


**Fig. S4** Simulation snapshots of NP spatial organizations in these systems with different content of B monomers: (a) 1.54%, (b) 3.07%, (c) 6.14%, and (d) 30.8%. The filler loading for each system was fixed at $\phi_{NP}$ = 11.62 vol%. In the snapshots, the cyan spheres, red spheres, and blue dots represent NPs, B monomers, and A monomers, respectively. (e) Radial distribution function of NPs, $g_{NP-NP}(r)$, and (f) the probability distribution of nearest neighbor coordination numbers (defined as number of NPs surrounding an NP at a separation closer than $4.5\sigma$), for systems at different $d_B$ but fixed filler loading of $\phi_{NP}$ = 11.62 vol%.

In addition, some simulations in which the B monomers were direct blending with polymer matrix were also carried out. The B monomers content is varied from $d_B$ = 1.54–30.8%. The

filler loading for each system was fixed at $\phi_{NP}$ = 11.62 vol%. The results show that no ordering can occur under such situations (Fig. S4a-d). The peaks appear at approximately $r = 4\sigma$ and $5\sigma$ in RDF (Fig. S4e) suggest two aggregation mechanisms of NPs: the directly connected of NPs and the bridging of NPs via monomers B, as schematically shown in Fig. S4e. With increasing $d_B$, more NPs are bridged via B monomers, as a consequence, the pairs of directly connected NPs decreased, which can be reflected from Fig. S4e (where the peaks at approximately $r = 4\sigma$ decreased but at approximately $r = 5\sigma$ increased) and Fig. S4f (where the number of nearest neighbors decreased). Particularly, for sufficiently high B monomer content ($d_B$ = 30.8%), all NPs are bridged via B monomers (Fig. S4d-f).

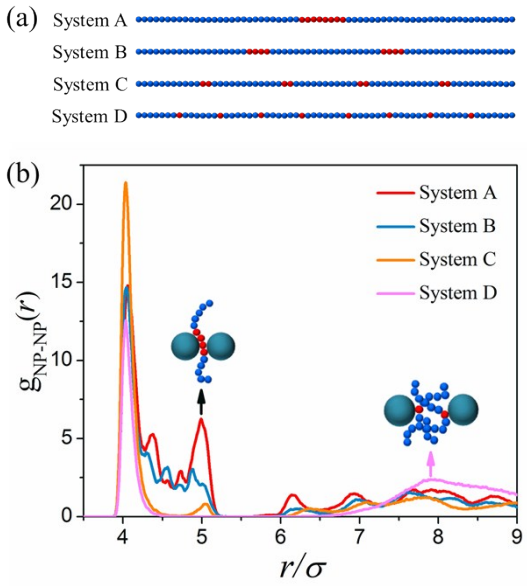


**Fig. S5** (a) Schematics for four systems with different distributions of B monomers in polymer chains. (b) The corresponding radial distribution functions of NPs, $g_{NP-NP}(r)$.

The above observations suggest that the connection of A and B monomers in polymer chains is important for the ordering of NPs. To further understand the role of the polymer backbones, four systems with different distributions of B monomers in polymer chains are constructed (Fig. S5a). For Systems A, B, and C, the NPs can aggregate through the bridging mechanism proposed

by Hooper and Schweizer,[13] i.e., the bridging of NPs via one layer of polymer chains (Fig. S5b). The longer the B blocks, the more NPs aggregated through bridging mechanism (Fig. S5b). This type of aggregation is absent in System D due to the steric crowding of A blocks in the chains, as schematically shown in Fig. S5b.

On the basis of the above analyses, we can find that in the systems with polymer chains of uniformly distributed B monomers, the role of the A blocks that connected to the B monomers is to prevent the aggregation of NPs in the region covered by B monomers, neither through direct connection of NPs nor through the bridging mechanism, i.e., the steric effect.

*Sizes and Numbers of Directly-Connected-NP Clusters*

Fig. S6 show that for $d_B$ fixed at 3.08% or lower, with increasing the filler loading, the clusters tend to combine into larger clusters (Fig. S6c), leading to the increase of the maximum cluster size (Fig. S6a) and the decrease of the cluster number (Fig. S6b), until all NPs are connected into one cluster. However, for higher $d_B$, with increasing the filler concentration, the cluster number first increases as sterically isolated NPs begin to coalesce into small clusters and then decreases when these small clusters further combine into several much larger clusters (finally into one cluster). For systems with $d_B$ = 30.8%, the NPs cannot connect into a major cluster to extend throughout the system, even at very high filler concentrations ($\phi_{NP}$ = 24.7%).

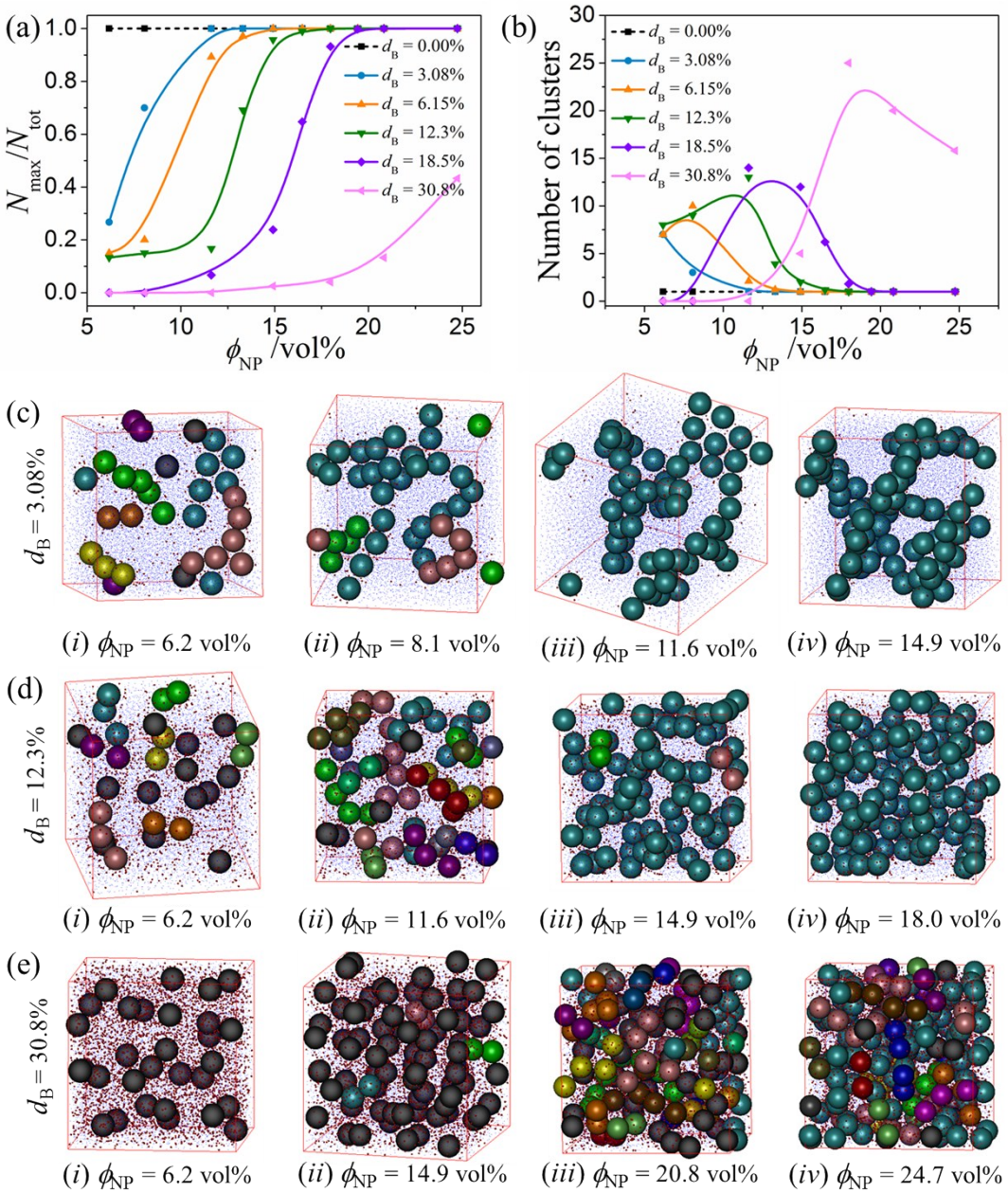


**Fig. S6** (a) Ratio of the number of NPs in the maximum cluster to the total number of NPs in the system ($N_{max}/N_{tot}$) and (b) number of clusters as a function of $\phi_{NP}$ and $d_B$. (c–e) Simulation snapshots of NP clustering states in systems with different filler loadings at three functionalization degrees: $d_B$ = 3.08%, 12.3%, and 30.8%. Black translucent spheres represent isolated NPs. Opaque spheres in other colors are used to denote clusters, where spheres with the same and different colors represent the NPs belonging to the same and different clusters, respectively. Light blue dots represent A monomers, and small red spheres denote B monomers. Because of the periodic boundary condition of the simulation box, one can see that some clusters are located in two or more sides of the box boundary region.

## References


1 K. Kremer and G. S. Grest, *J. Chem. Phys.,* 1990, **92**, 5057.

2 J. S. Smith, D. Bedrov and G. D. Smith, *Compos. Sci. Technol.,* 2003, **63**, 1599.

3 S. Plimpton, *J. Comput. Phys.,* 1995, **117**, 1.

4 D. J. Evans and G. P. Morriss, In *Statistical Mechanics of Nonequilibrium Liquids*, Academic Press, London, 1990, pp 328.

5 M. E. Tuckerman, C. J. Mundy, S. Balasubramanian and M. L. Klein, *J. Chem. Phys.,* 1997, **106**, 5615.

6 C. M. Tenney and E. J. Maginn, *J. Chem. Phys.,* 2010, **132**, 014103.

7 C. Bennemann, W. Paul, J. Baschnagel and K. Binder, *J. Phys.: Condens. Matter,* 1999, **11**, 2179.

8 C. Bennemann, W. Paul, K. Binder and B. Dünweg, *Phys. Rev. E*, 1998, **57**, 843.

9 C. Bennemann, J. Baschnagel and W. Paul, *Eur. Phys. J. B*, 1999, **10**, 323.

10 Y. Lu, L. An, S.-Q. Wang and Z.-G. Wang, *ACS Macro Lett.*, 2014, **3**, 569.

11 J. Liu, D. Cao and L. Zhang, *J. Phys. Chem. C*, 2008, **112**, 6653.

12 D. Long and P. Sotta, *Macromolecules,* 2006, **39**, 6282.

13 J. B. Hooper and K. S. Schweizer, *Macromolecules*, 2005, **38**, 8858.

14 J. Liu, Y. Gao, D. Cao, L. Zhang and Z. Guo, *Langmuir,* 2011, **27**, 7926.

15 Y. Chen. L. Liu, Q. Yang, S. Wen, L. Zhang and C. Zhong, *Langmuir,* 2013, **29**, 13932.